Impaired Hippocampal Reactivation Preceding Robust Aβ Deposition in a Model of Alzheimer's Disease

Hanyan Li [1,2,*], Zhuoyang Zhao [1,2,*], Aline Fassini [1,2], Han K. Lee [1,2], Reese J. Green [1,2], and Stephen N. Gomperts [1,2,#]

* Contributed equally to this work

[1] Department of Neurology, Massachusetts General Hospital, Boston, Massachusetts, USA.

[2] Harvard Medical School, Boston, Massachusetts, USA.

Correspondence should be addressed to SNG at Gomperts.stephen@mgh.harvard.edu

Abstract

Current therapeutic strategies for Alzheimer's disease (AD) target amyloid-beta (Aβ) fibrils and high molecular weight protofibrils associated with plaques, but other bioactive species may directly contribute to neural systems failure in AD. Employing hippocampal electrophysiological recordings and dynamic calcium imaging across the sleep-wake cycle in young mice expressing human Aβ and Aβ oligomers, we reveal marked impairments of hippocampal function long before amyloid plaques predominate. In slow wave sleep (SWS), Aβ increased the proportion of hypoactive cells and reduced place-cell reactivation. During awake behavior, Aβ impaired theta-gamma phase-amplitude coupling (PAC) and drove excessive synchronization of place cell calcium fluctuations with hippocampal theta. Remarkably, the on-line impairment of hippocampal theta-gamma PAC correlated with the SWS impairment of place-cell reactivation. Together, these results identify toxic effects of Aβ on memory encoding and consolidation processes before robust plaque deposition and support targeting soluble Aβ-related species to treat and prevent AD.

Introduction

In Alzheimer's disease (AD), deposition of amyloid-beta42 (Aβ) in amyloid plaques and aggregation of intracellular tau in neurofibrillary tangles are associated with neuronal loss and progressive memory impairment on the basis of hippocampal systems failure [1]. The advent of amyloid-targeted immunotherapies such as Lecanemab (targeting high molecular weight Aβ protofibrils as well as fibrils in plaques) [2], Donanemab (targeting the pyroglutamate modification seen in Aβ fibrils in plaques) [3], and Aducanumab (targeting Aβ fibrils in plaques) [4] for the treatment of AD heralds the beginning of a new era, with evidence to date demonstrating marked reductions of brain amyloid. Even so, these treatments as yet have only modestly improved cognitive outcomes of AD patients [2,3,5]. Several plausible explanations may explain this discrepancy, including the possibility that these state-of-the-art treatments do not adequately target an unknown but key element underlying Aβ's toxicity.

Much is known about the deleterious effects of Aβ amyloidosis on hippocampal function. During online memory encoding processes, hippocampal place cells form place fields that are activated sequentially as animals explore an environment in coordination with the hippocampal theta oscillation [6,7]. In Aβ plaque-bearing mice, place representations [8,9] and the coupling of the amplitude of gamma oscillations to the phase of theta [10–17] are impaired, and hyper-synchronization of neuronal calcium fluctuations with the theta oscillation has been observed [18]. Aβ plaque-bearing mice also show impaired off-line hippocampal memory consolidation processes: In SWS, reduced reactivation of hippocampal place cell ensembles [19] and reduced coordination of hippocampal sharp wave ripples (SWRs) with cortical spindles and slow oscillations in SWS [18,20]; in REM sleep,

reduced theta-gamma coupling [18,21,22], as well as hyper-synchronization of neuronal calcium fluctuations with the theta oscillation [18].

In contrast, few studies have examined plaque-independent toxicity of Aβ on hippocampal systems function. Soluble species of Aβ that predominate before plaques form may contribute to this toxicity. Among these, soluble Aβ oligomers (AβO) have been suggested to confer significant cytotoxicity and have been shown to impair synapse function, plasticity, and density [23–33] and to drive hippocampal neuronal hyper-excitability in anesthetized AD models [34–36]. To evaluate whether Aβ amyloidosis can impair hippocampal physiology crucial to memory encoding and consolidation before plaques predominate, here we acquired and compared hippocampal dynamic calcium imaging and hippocampal and cortical electrophysiological recordings in freely-behaving, young APPswe/PS1dE9 (APP/PS1) transgenic mice and their littermate controls, at an age when soluble AβOs are present but before Aβ plaques predominate [37,38]. We found marked impairments of hippocampal memory encoding and consolidation processes even before robust plaque deposition.

Results

To evaluate the effects of early Aβ amyloidosis on hippocampal function, we acquired hippocampal CA1 dynamic calcium imaging with GCaMP6f using the Inscopix miniscope™ together with simultaneous cortical and hippocampal local field potential (LFP) recordings of young APP/PS1 mice (5.2 ± 0.6 months, n=8, male) and their littermate controls (4.7 ± 0.5 months, n=7, male; age, $p > 0.05$, 2-sided t-test), as animals explored a linear track (RUN) and subsequently rested and slept (Fig. 1a).

83

84 **Soluble Aβ oligomers and a minimal burden of Aβ plaques in young Aβ mice**

85 In the APP/PS1 model, Aβ plaques have been reported to first deposit around 6 months [37,38] and
86 levels of soluble AβO increase with age [39,40]. Consistent with these reports, we observed few Aβ
87 plaques in hippocampus and cortex in APP/PS1 mice in this age range compared to 12-month-old
88 positive control mice (hippocampus: repeated measures ANOVA $F(4,15)=42.1$, $p<0.001$, post hoc
89 comparison with positive control $p<0.001$; cortex: repeated measures ANOVA $F(4,15)=105.4$,
90 $p<0.001$, post hoc comparison with positive control $p<0.001$, Fig. 1b, c). Soluble AβO was
91 detected in both hippocampus and cortex and increased with age (hippocampus $R=0.5$, $p=0.03$;
92 cortex $R=0.6$, $p=0.006$, Pearson correlations, Fig. 1d).

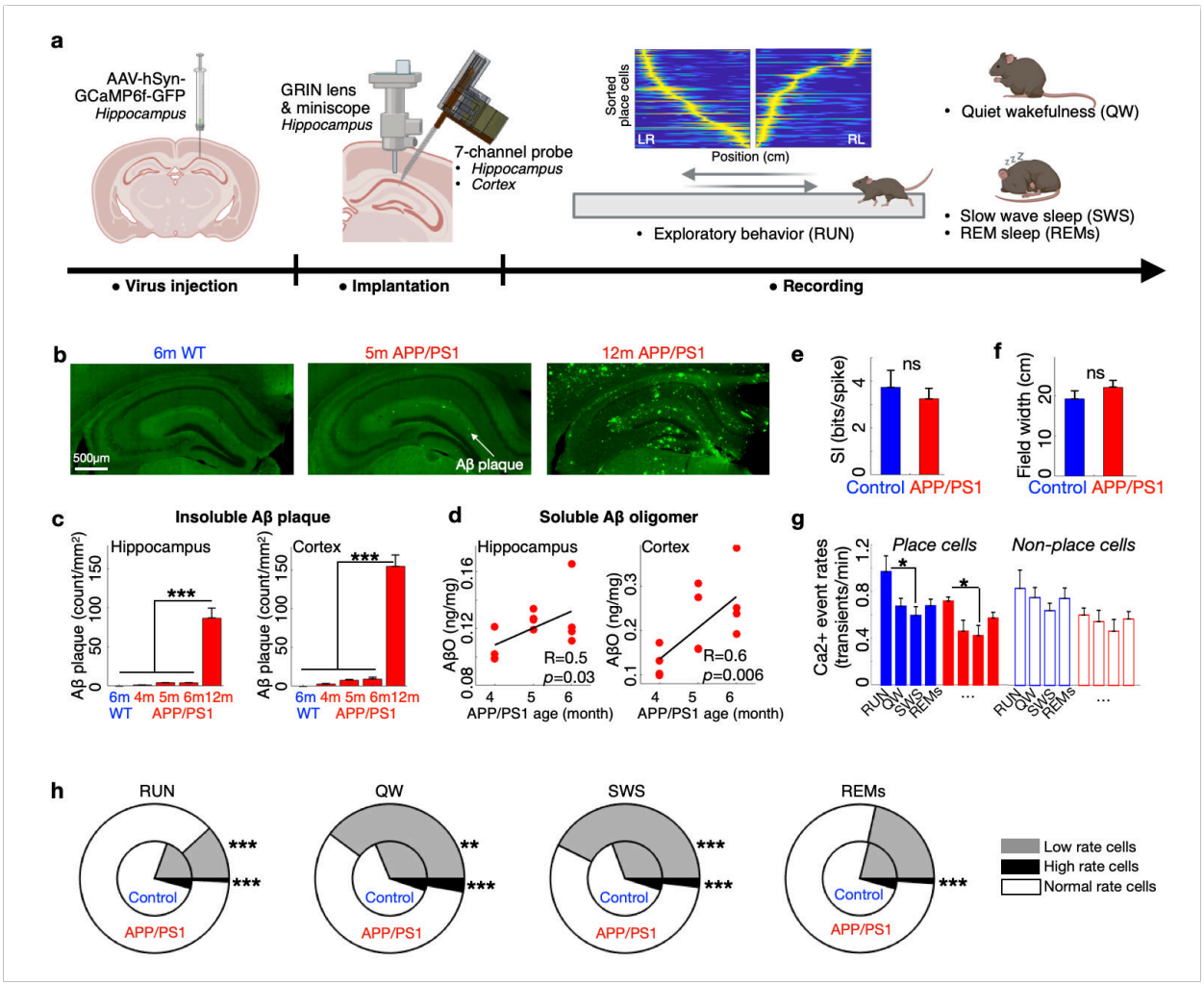

Figure 1. Young APP/PS1 mice harboring soluble AβO but minimal Aβ plaque counts showed preserved place cell function and reduced calcium activity. a) *Schematic of hippocampal calcium imaging and simultaneous ipsilateral LFP recording across the sleep-wake cycle: exploratory behavior (RUN), insert: example of place cells sorted by their place fields (in yellow) in inbound (LR) and outbound (RL) directions. Yellow shows the place field of each cell; quiet wakefulness (QW); slow wave sleep (SWS) and rapid eye movement (REM) sleep.* ***b)*** *Immunohistochemistry against Aβ in hippocampus of a wild-type control mouse (6 months) and APP/PS1 mice at 5 and 12 months. Green: Aβ plaques (D54D2).* ***c)*** *Aβ plaque counts in hippocampus and cortex were low in 4-6 month-old APP/PS1 mice and increased markedly at 12 months.* ***d)*** *Level of soluble AβO in hippocampus and cortex increased with age in APP/PS1 mice.* ***e)*** *Spatial information (SI) and* ***f)*** *place field width were comparable across genotypes.* ***g)*** *Calcium event rates of place cells and non place cells in each behavioral state were similar to those of littermate control mice, and calcium event rates of place cells were higher in RUN than SWS in both genotypes.* ***h)*** *In RUN and REM sleep, APP/PS1 had fewer low rate and high rate cells; In QW and SWS, APP/PS1 had more low rate cells and fewer high rate cells. * p<0.05, ** p<0.01, ***p<0.001; c, g, ANOVA with post-hoc comparisons; e, f, 2-sided t-test; d, Pearson correlation; h, mixed effects model. b-c: each group*

n=4 mice; e-h: Control n=5 mice, 395 place cells, 2169 total cells; APP/PS1 n=6 mice, 237 place cells, 2133 total cells. Data are represented as mean ± S.E.M.

Young Aβ mice showed intact place representations but reduced dynamic calcium activity across behavioral states

Behavior was comparable across young APP/PS1 and littermate control groups, with similar run velocity (Control: 4.1 ± 0.7 cm/s; APP/PS1: 3.5 ± 0.6 cm/s, p>0.05, 2-sided t-test) and laps on the track (Control: 34.2 ± 3.2 laps; APP/PS1: 39.8 ± 2.5 laps, p>0.05, 2-sided t-test), consistent with prior reports [41].

We next investigated place cell representations across the genotypes. As place fields are often directional, we separated inbound (LR) and outbound (RL) trajectories (Fig. 1a insert). The proportion of place cells was similar in APP/PS1 and control mice (Control: 16.8% ± 1.9%; APP/PS1: 11.0% ± 2.1%. p=0.07, 2-sided t-test). Spatial information (p>0.05, 2-sided t-test, Fig. 1e) and place field width (p>0.05, 2-sided t-test, Fig. 1f) were also similar across the genotypes. These results are consistent with prior work [42].

Previous studies in plaque-laden anesthetized and freely behaving AD models have detected aberrant neuronal activity [18,34,35], and studies in young anesthetized AD mice [34,36] have reported hyperactivity of hippocampal neurons that has been suggested to precede amyloid plaque formation. We therefore extended analyses of neuronal activity across the sleep-wake cycle of young, freely behaving AD mice. In the young APP/PS1 mice studied here, place cell (and nonplace cell) mean calcium event rates in each behavioral state were similar to those of littermate control mice (p>0.05, 2-sided t-tests, Fig. 1g). Consistent with prior results in plaque-laden AD

135 models [18], calcium event rates of place cells were higher in RUN than in SWS in both APP/PS1
136 and control mice (Control: repeated measures ANOVA: $F(3,16)=3.46$, $p=0.04$, post hoc
137 comparison: RUN vs SWS, $p=0.03$; APP/PS1: repeated measures ANOVA: $F(3,20)=3.57$, $p=0.03$,
138 post hoc comparison: RUN vs SWS, $p=0.003$, Fig. 1g). In both APP/PS1 and control mice, the
139 calcium event rates of non-place cells were similar across behavioral states.
140
141 In contrast to previous findings once Aβ plaques predominate, including hyperactivity in RUN and
142 SWS, and hypoactivity in QW and REM sleep [18], here prior to robust Aβ deposition, we found no
143 hyperactivity (> 2SD above mean in control group [18]) in any behavioral state (high rate cell
144 proportions, Control vs APP/PS1, RUN: 4.2% ± 0.4% vs 0.7% ± 0.6%, $p<0.001$; QW: 5.1% ± 0.4%
145 vs 2.8% ± 1.9%, $p=0.001$; SWS: 4.9% ± 0.3% vs 1.8% ± 1.5%, $p<0.001$; REM sleep: 4.4% ± 0.5%
146 vs 1.0% ± 0.8%, $p<0.001$. Mixed effects model, Fig 1h). Instead, we observed an increased
147 proportion of hypoactive cells (< 0.25 spikes/min [18,34]) in QW and SWS (low rate cell proportions,
148 Control vs APP/PS1, RUN: 19.5% ± 8.2% vs 11.7% ± 1.5%, $p<0.001$; QW: 31.2% ± 4.7% vs 39.8%
149 ± 5.8%, $p=0.009$; SWS: 30.6% ± 3.5% vs 42.5% ± 11.5%, $p<0.001$; REM sleep: 21.0% ± 4.0% vs
150 21.5% ± 3.5%, ns. Mixed effects model, Fig 1h), regardless of place cell identity.
151
152 **Reduced place cell reactivation despite intact oscillations of slow wave sleep in young Aβ mice**
153 Since place cell properties of young Aβ mice were essentially intact at the single cell level, we
154 next evaluated place cell coordination in offline behavioral states. Building on the observation that
155 place cells that fire together online during exploratory behavior tend to fire together during
156 subsequent rest and sleep in the service of memory consolidation [43–45], and on prior work showing
157 that Aβ plaque-bearing mice have fewer and shorter SWRs in conjunction with reduced place cell

158 reactivation in SWS [19], we set out to evaluate place cell offline reactivation prior to robust Aβ
159 plaque deposition. SWR frequency and duration were comparable in young APP/PS1 and control
160 mice (SWR rate: Control 0.06 ± 0.01 event/s; APP/PS1 0.08 ± 0.02 event/s; duration: Control
161 0.024 ± 0.0005 s; APP/PS1 0.025 ± 0.0006 s; $p>0.05$, 2-sided t-tests). We calculated the spike time
162 cross-correlation of all place cell pairs during exploratory behavior (RUN) and in subsequent
163 offline states, and defined reactivation when a place cell pair was coactive in both online and
164 offline states [45] (Fig. 2a, see Methods and Fig. S1). Pairwise reactivation was confirmed in each
165 genotype by comparing to the distribution of 500 cross-correlations of shuffled spike times
166 (Supplementary Fig. S2a). Despite similar numbers and firing rate of place cells in APP/PS1 and
167 control mice (see above), the percentage of place cell pairs that reactivated in SWS was
168 significantly reduced in APP/PS1 compared to control mice ($p=0.005$, $T=3.6$, $df=9$, 2-sided t-test,
169 Fig. 2a, b). This difference persisted after matching place cell firing rate and place cell numbers in
170 control mice to APP/PS1 mice (Supplementary Fig. S2b-d). Differential pairwise reactivation
171 between APP/PS1 and control mice was not detected in QW or REM sleep ($p>0.05$, 2-sided t-test,
172 Fig 2a, b). Thus, hippocampal reactivation necessary for memory consolidation in SWS was
173 reduced in young APP/PS1 mice prior to robust Aβ plaque deposition.

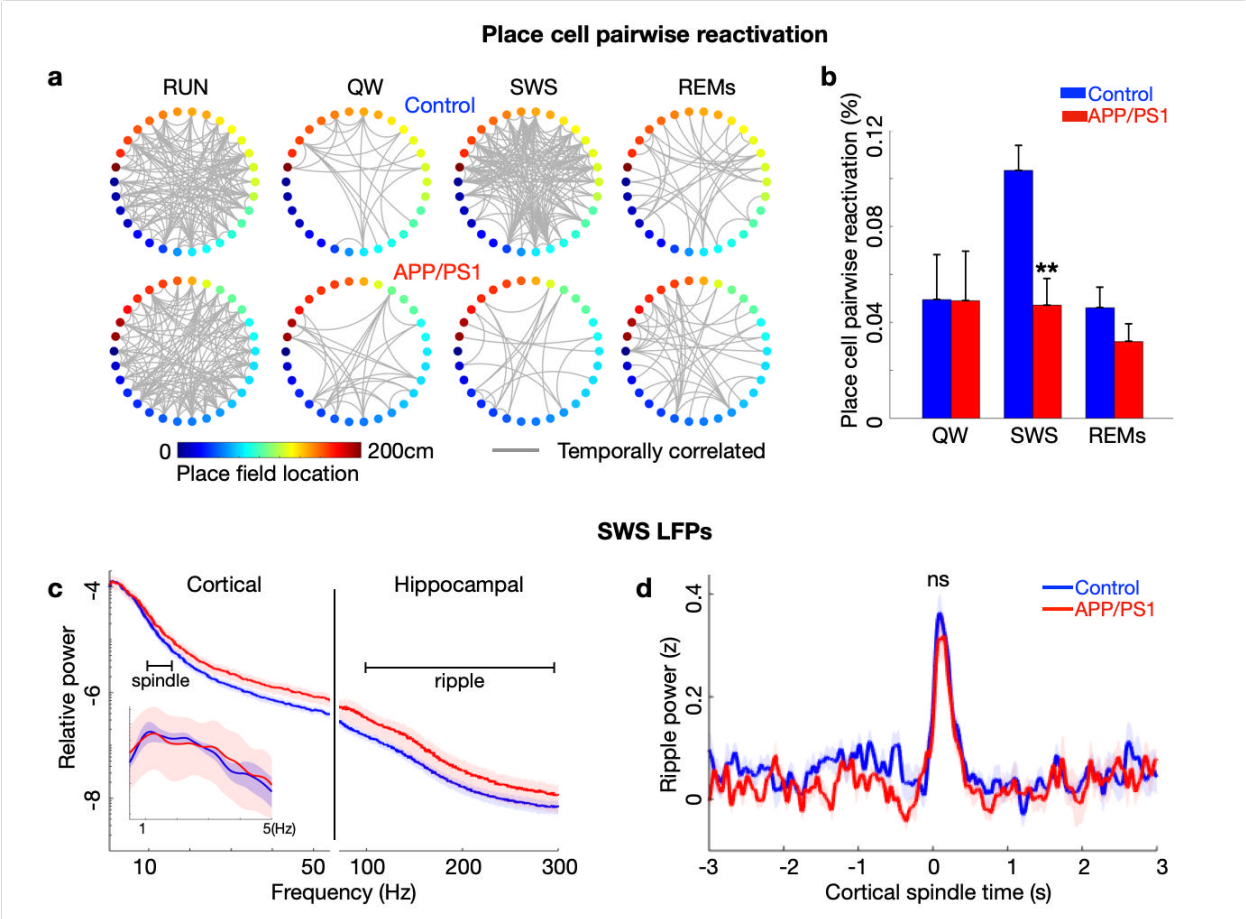

Figure 2. Young APP/PS1 mice showed reduced place cell pairwise reactivation but intact oscillations of slow wave sleep. a) *Spike time cross-correlations of 30 randomly selected place cells from one control and one APP/PS1 mouse, sorted by place field location on the track (colorbar). Grey line: coactivation.* ***b)*** *The percentage of place cell pairs that were temporally reactivated in slow wave sleep (SWS) was reduced in APP/PS1 compared to control mice, but not in QW or REM sleep.* ***c)*** *In SWS, power in the cortical SO, delta, spindle and hippocampal ripple bands was comparable between genotypes. Insert: cortical slow oscillation and delta power.* ***d)*** *Cortical spindle-triggered ripple power was comparable between genotypes. **$p < 0.01$, 2-sided t-tests. Control n=5 mice, 395 place cells, 2169 total cells; APP/PS1 n=6 mice, 237 place cells, 2133 total cells. Data are represented as mean ± S.E.M.*

To investigate possible mechanisms underlying the reduction of APP/PS1 place cell reactivation in SWS, we next evaluated the coordination of the signature hippocampal and cortical oscillations of SWS. Hippocampal SWRs, cortical spindles, cortical slow oscillations and their nested coordination are fundamental features of slow wave sleep [46] that contribute to memory

consolidation [47]. These oscillations and their coordination are degraded in Aβ plaque-bearing AD models [18,20]. However, in young APP/PS1 mice harboring abundant soluble AβO prior to robust Aβ plaque deposition, we found that the oscillations of SWS and their coordination remained intact. Specifically, SWR rates and duration (see above), cortical SO power, cortical spindle power, and hippocampal ripple power ($p>0.05$, 2-sided t-tests, Fig. 2c) were comparable between APP/PS1 and control mice, and the coordination of cortical spindles with hippocampal ripples was similar across genotypes ($p>0.05$, 2-sided t-test, Fig. 2d). Together, these results show that the characteristic hippocampal and cortical oscillations of SWS remain intact at this early stage of Aβ amyloidosis and dissociate from the reduction of APP/PS1 place cell pairwise reaction.

In young Aβ mice, online theta-gamma coupling was impaired, decreased with age, and correlated with offline place cell reactivation

Since the physiologic oscillations of SWS were intact in young APP/PS1 mice, we next examined whether the reduction in place cell pairwise reactivation observed in SWS could be predicted by changes in online oscillatory physiology linked to memory encoding. Intra-hippocampal and hippocampal-cortical theta-gamma phase amplitude coupling (PAC) both contribute to memory encoding [11,22] and have been reported to degrade in Aβ plaque-bearing AD models [9,18,48–51]. Hippocampal theta and gamma power were comparable across young APP/PS1 and control mice ($p>0.05$, 2-sided t-tests, Fig 3a), and, as noted above, running behavior was comparable across genotypes. However, intra-hippocampal theta (6-8 Hz) -gamma (40-80 Hz) PAC was impaired in young APP/PS1 mice ($p=0.03$, $T=2.3$, $df=13$, 2-sided t-test, Fig. 3b). In contrast to control mice, hippocampal theta-gamma PAC in APP/PS1 mice was negatively correlated with age ($R=-0.7$,

213 p=0.02, Pearson correlation, Fig. 3c). These results were unchanged after controlling for the
214 possible contribution of theta harmonics [10] (Supplementary Fig. S3 a-c).
215
216 Cortical gamma power was also comparable between genotypes (p>0.05, 2-sided t-tests, Fig. 3d),
217 yet hippocampal theta (6-8 Hz) - cortical gamma (40-80 Hz) PAC was also impaired in young
218 APP/PS1 (p=0.02, T=2.5, df=13, 2-sided t-test, Fig. 3e). As with intrahippocampal theta-gamma
219 PAC, in APP/PS1 but not control mice, hippocampal-cortical PAC was negatively correlated with
220 age (R=-0.8, p=0.007, Pearson correlation, Fig. 3f). As above, these results persisted after
221 controlling for the possible contribution of theta harmonics [10] (Supplementary Fig. S3 d-f). As
222 soluble AβO levels increase with age (Fig. 1c and [39,40]), these results suggest that theta-gamma
223 PAC during exploratory behavior falls with progression of amyloidosis, prior to robust plaque
224 deposition.
225
226 Interestingly, the extent of place cell pairwise reactivation in SWS of young APP/PS1 mice was
227 strongly and significantly correlated with the magnitude of hippocampal theta-gamma PAC in
228 RUN (R=0.8, p=0.02, Pearson correlation, Fig. 3g) but was not correlated with age (p>0.05, Fig.
229 3h). Together, these observations suggest that the impairment of theta-gamma PAC underlying
230 memory encoding evident prior to robust Aβ plaque deposition may serve as a proximal driver of
231 the impairment of place cell pairwise reactivation necessary for memory consolidation in SWS.
232
233 As oscillations both coordinate and reflect the coordination of neuronal activity, and as calcium
234 signaling links synaptic activity to synaptic plasticity and gene expression, we considered the
235 possibility that a breakdown in the coordination of neuronal activity reflected in impaired theta-

236 gamma PAC might manifest at the cellular level in altered coordination of somatic calcium
237 fluctuations with the LFP. In exploratory behavior, neuronal calcium levels can synchronize with
238 theta oscillations, and prior work has shown that such synchronization is aberrantly increased in
239 aged Aβ plaque-bearing mice [18]. To determine if hyper-synchronization arises in early amyloidosis
240 prior to robust plaque deposition, we evaluated the coherence of hippocampal neuronal calcium
241 traces with the hippocampal LFP in young APP/PS1 mice. Compared to control mice, young
242 APP/PS1 mice showed hyper-synchronization of place cell calcium fluctuations with theta
243 (repeated measures ANOVA: $F(3,16)=4.5$, $p=0.01$, post-hoc comparison: control vs APP/PS1,
244 place cells, $p=0.02$; nonplace cells, $p>0.05$; Fig. 3i). Thus, even before robust Aβ plaque deposition,
245 dysfunctions of memory encoding processes at both the oscillatory and the cellular level are readily
246 detected in APP/PS1 mice.
247

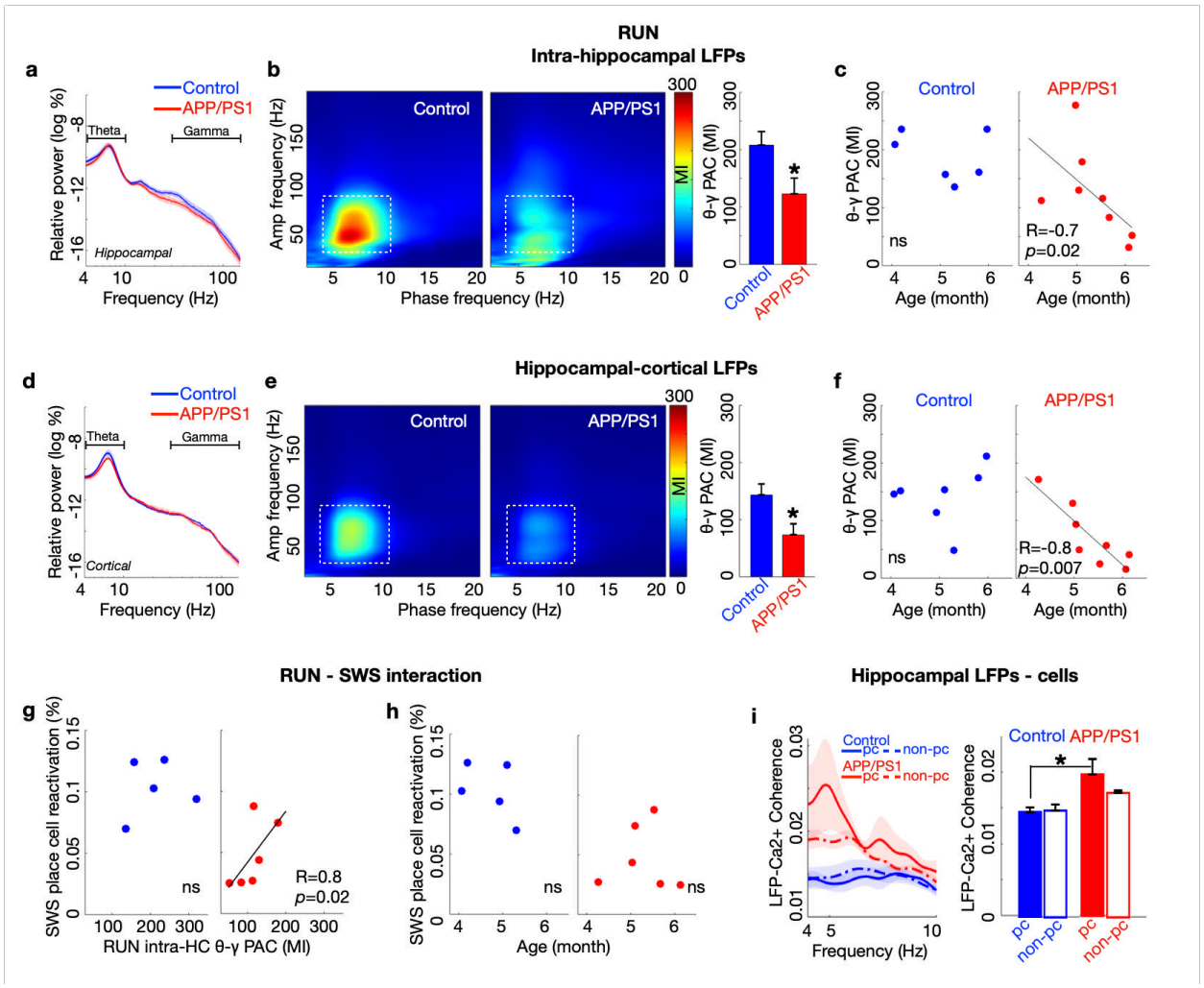

Figure 3. In young APP/PS1 mice, online theta-gamma coupling was impaired, decreased with age, and correlated with offline place cell reactivation. a) *In RUN, hippocampal theta and gamma power in APP/PS1 and control mice were comparable.* ***b)*** *Intra-hippocampal theta (6-8Hz) - gamma (40-80Hz) phase - amplitude coupling (PAC) was reduced in APP/PS1 compared to control mice.* ***c)*** *Intrahippocampal theta-gamma PAC was negatively correlated with the age of APP/PS1 mice but not control mice.* ***d)*** *Cortical gamma power was comparable between genotypes.* ***e)*** *PAC of hippocampal theta (6-8Hz) - cortical gamma (40-80Hz) was reduced in APP/PS1 compared to control mice.* ***f)*** *The reduction of hippocampal theta- cortical gamma PAC was negatively correlated with age in APP/PS1 but not control mice.* ***g)*** *In APP/PS1 but not controls, the extent of place cell pairwise reactivation in SWS correlated with the magnitude of intra-hippocampal theta-gamma PAC in RUN.* ***h)*** *The proportion of reactivated place cell pairs in SWS was not correlated with age.* ***i)*** *Average theta-range oscillatory-cellular coherence of place cells was higher in APP/PS1 than control mice. *p < 0.05; b, e, 2 sided t-test; c, f, g, Pearson correlation; i, ANOVA with post-hoc comparisons. a – f: Control n=7 mice, APP/PS1 n=8 mice; g – i: Control n=5 mice, 395 place cells, 1774 non-place cells, 2169 total cells; APP/PS1 n=6 mice, 237 place*

cells, 1896 non-place cells, 2133 total cells. Data are represented as mean ± S.E.M. pc, place cells. Non-pc, nonplace cells.

In young Aβ mice, offline theta-gamma coupling was intact but decreased with age

As intra-hippocampal and hippocampal-cortical theta-gamma PAC in REM sleep contribute to memory consolidation [52,53] and are diminished in Aβ plaque-bearing AD mice [18,50], we next evaluated REM sleep theta-gamma PAC prior to robust Aβ plaque deposition. Hippocampal REM sleep theta and gamma power ($p>0.05$, 2-sided t-test, Fig. 4a), and intra-hippocampal theta (6-8 Hz) -gamma (40-80 Hz) PAC were comparable across genotypes ($p>0.05$, 2-sided t-test, Fig. 4b), consistent with prior results [50]. Although a trend level correlation between intra-hippocampal PAC magnitude and the age of APP/PS1 mice was observed ($R=-0.6$, $p=0.05$, Pearson correlation, Fig. 4c), this result did not survive after controlling for the possible contribution of theta harmonics (Supplementary Fig. S4 a-c).

REM sleep cortical gamma power ($p>0.05$, 2-sided t-test, Fig. 4d), and hippocampal theta (6-8 Hz) – cortical gamma (40-80 Hz) PAC were also comparable across genotypes ($p>0.05$, 2-sided t-test, Fig. 4e). Even so, in APP/PS1 but not control mice, hippocampal-cortical PAC in REM sleep was significantly and negatively correlated with age ($R=-0.8$, $p=0.005$, Pearson correlation, Fig. 4f), and this result persisted after controlling for the possible contribution of theta harmonics (Supplementary Fig. S4 d-f). Accumulation of soluble AβO levels with age (Fig. 1c and [37,39]) may contribute to this age-dependent reduction in REM sleep hippocampal theta - cortical gamma PAC.

Because theta-gamma PAC in APP/PS1 mice was differentially affected in RUN and REM sleep but negatively correlated with age in both behavioral states, we next evaluated how theta-gamma PAC in RUN and REM sleep related to one another. There was a trending correlation between the

magnitude of intra-hippocampal theta-gamma PAC in RUN and REM sleep in both APP/PS1 and control mice (Control R=0.6, p=0.05; APP/PS1 R=0.5, p=0.06; Pearson correlations, Fig. 4g), while the magnitude of hippocampal theta - cortical gamma PAC in RUN and in REM sleep were significantly correlated in both genotypes (Control R=0.9, p=0.001; APP/PS1 R=0.6, p=0.04; Pearson correlation, Fig 4h).

We next sought to evaluate whether the hyper-synchronization of somatic calcium levels with the theta oscillation that we observed in exploratory behavior (Figure 3i) extended to REM sleep. In contrast to findings in exploratory behavior, in REM sleep neuronal calcium synchronization with theta was similar across APP/PS1 and control mice ($p>0.05$, 2-sided t-tests, repeated measures ANOVA, Fig. 4i). Thus, although theta-gamma PAC in REM sleep decreased with age in young APP/PS1 mice, neither theta-gamma PAC nor the coherence of neuronal calcium with the theta oscillation in REM sleep was altered. These results suggest that REM sleep may be more resilient to the effects of Aβ at a stage when soluble Aβ species predominate and the extent of plaque deposition is low.

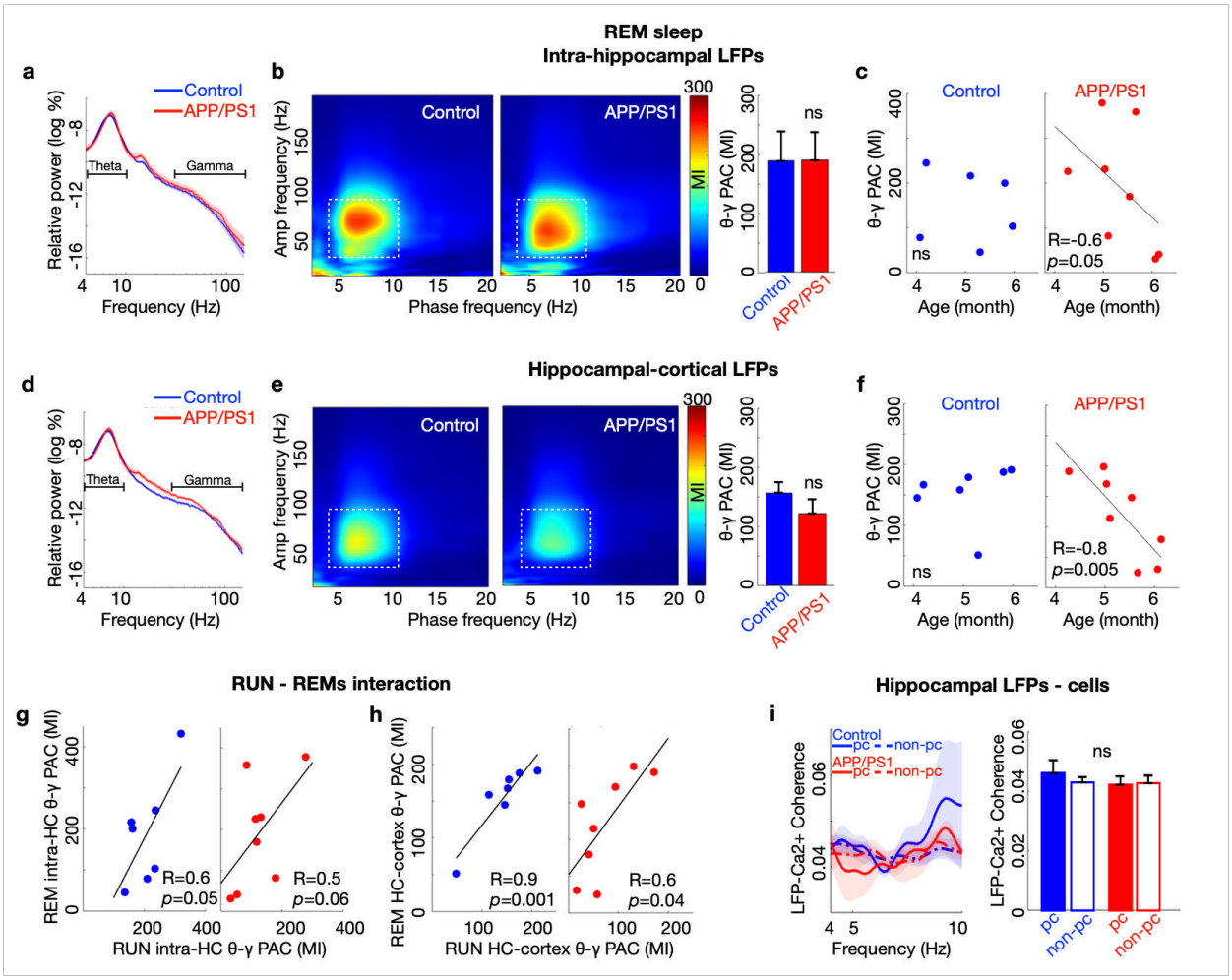

Figure 4. In young APP/PS1 mice, theta-gamma coupling in REM sleep was intact, decreased with age, and correlated with online theta-gamma coupling. a) *In REM sleep, hippocampal spectral power, and* ***b)*** *intra-hippocampal theta (6-8Hz) - gamma (40-80Hz) phase-amplitude coupling (PAC) were comparable in APP/PS1 and control mice.* ***c)*** *Intrahippocampal theta-gamma PAC showed a trending negative correlation with the age of APP/PS1 mice but not control mice.* ***d)*** *Cortical spectral power, and* ***e)*** *PAC of hippocampal theta (6-8Hz) - cortical gamma (40-80Hz) were comparable across genotypes.* ***f)*** *Hippocampal theta- cortical gamma PAC was negatively correlated with age in APP/PS1 mice but not control mice.* ***g)*** *Intra-hippocampal theta-gamma PAC between RUN and REM sleep showed a trending correlation in both genotypes.* ***h)*** *Hippocampal theta - cortical gamma PAC in RUN and in REM sleep were significantly correlated in both AP/PS1 and control mice.* ***i)*** *Average theta-range oscillatory-cellular coherence in REM sleep was comparable across APP/PS1 and control mice. b, e, 2 sided t-test; c, f, g, h, Pearson correlation; i, ANOVA with post-hoc comparisons. a – g: Control n=7 mice, APP/PS1 n=8 mice; i: Control n=5 mice, 395 place cells, 2169 total cells; APP/PS1 n=6 mice, 237 place cells, 2133 total cells. Data are represented as mean ± S.E.M. pc, place cells. Non-pc, nonplace cells.*

Discussion

We investigated hippocampal functions related to memory encoding and consolidation across the sleep wake cycle in APP/PS1 mice at an early stage when soluble Aβ was present and plaque counts were low. We found reduced place cell reactivation in SWS that correlated with the extent of impairment in theta-gamma PAC during online exploratory behavior, together with excessive on-line theta synchronization of hippocampal place cells with their surrounding local field potential. Together, these results show that even in the absence of significant plaque burden, Aβ is highly toxic to hippocampal functions that link online memory encoding to offline memory consolidation.

While tau fibrils and neuronal loss are strong predictors of cognitive impairment in AD [54,55], the impact of other AD-associated processes such as accumulating AβO on cognitive functions has received less recent attention. Even so, AβOs are well-known to be cytotoxic and have been shown to induce cognitive impairment in vitro and in vivo [28,33,56]. They interact with glutamate receptors, prion protein, neuroligin, the frizzled receptor and other partners [28], bind to synapses promoting structural modifications, reduce dendritic spine density in hippocampus [31] leading to synaptic dysfunction and loss [23–30], and disrupt and bias synaptic plasticity [28,32,33]. In addition, in contrast to Aβ plaque counts, levels of soluble Aβ species have been shown to correlate with reduced synapse density in AD brain tissue and to differentiate AD dementia cases from cognitively normal cases harboring high levels of plaques and tangles [57]. Among soluble Aβ species, small oligomers are particularly toxic [33], and levels of small brain Aβ oligomers but not monomer have been shown to correlate with AD progression in APP/PS1 mice at 3 – 9 months of age [40].

347 Given AβO's cellular and synaptic toxicity and relevance to AD progression, as well as the minimal
348 levels of Aβ protofibrils detectable in young APP/PS1 mice [40], the accumulation of AβOs is well-
349 positioned to contribute to the marked systems-level hippocampal dysfunctions observed here in
350 young APP/PS1 mice. Future causal experiments will be of value to test this possibility and to
351 evaluate the contribution of other APP digestion products or PS1 substrates [58,59] to the current
352 findings. Together with the significant but modest effectiveness of Lecanemab, Donanemab, and
353 Aducanumab in improving cognitive function in Alzheimer's patients despite robust reduction of
354 amyloid plaque burden, and the lack of efficacy seen in targeting Aβ monomers with Solanezumab
355 [5], the present results draw attention to the therapeutic potential of targeting extra-plaque, small
356 oligomeric species that predominate in early amyloidosis to treat and prevent AD.
357
358 Surprisingly, despite observing marked abnormalities of hippocampal function across the sleep-
359 wake cycle of young APP/PS1 mice, we did not detect aberrant neuronal hyperactivity, as has been
360 reported in anesthetized AD models [34,35]. This discrepancy suggests that in the freely-behaving
361 animal, hippocampal dynamic calcium hyperactivity does not appear to be a prominent finding of
362 early Aβ pathology.
363
364 Hippocampal place cells encode the environment during online behavior, and their network
365 reactivation during offline behaviors, including hippocampal replay during sharp wave ripples [43,60],
366 contributes to sleep-dependent learning [43,61] and memory consolidation [44,62,63]. Prior work has
367 reported reduced place cell reactivation in Aβ plaque bearing mice [19], and the present results show
368 that this result persists at an earlier stage of amyloidosis when plaques are sparse. The impairment
369 of pair-wise reactivation did not arise from differences in behavior, ripple features, or place cell

370 properties between young APP/PS1 and control mice. Likewise, although the coordination of
371 cortical slow oscillations, corticothalamic spindles, and hippocampal sharp wave ripples is a key
372 feature of memory consolidation in SWS [46,47], and this coordination degrades in Aβ plaque-bearing
373 animals [18,20], these oscillations and their coordination remained intact in young APP/PS1 mice. As
374 such, the reduced pairwise reactivation observed in SWS in these mice identifies an impairment in
375 memory consolidation mechanisms prior to, and in the absence of, breakdown of SWS oscillatory
376 coordination.
377
378 Brain oscillations and their coupling play a crucial role in hippocampal-dependent memory
379 functions. Online intra-hippocampal and hippocampal-cortical theta-gamma phase-amplitude
380 coupling (PAC) have been linked to memory encoding [10–17], and, like the coordinated oscillations
381 of SWS, are also impaired in multiple AD models harboring Aβ plaques [9,18,48–51]. In contrast to the
382 preserved oscillations of SWS, online hippocampal and hippocampal-cortical theta-gamma PACs
383 were reduced in young APP/PS1 mice. As the extent of these reductions correlated with age, online
384 theta-gamma PAC appears to degrade as amyloidosis progresses, potentially on the basis of the
385 accumulation of AβO or other species.
386
387 The intra-hippocampal and hippocampal-cortical theta-gamma PACs of REM sleep have also been
388 linked to memory consolidation [10,11] , and these deteriorate in plaque-bearing AD model mice [18].
389 However, in young APP/PS1 mice, theta-gamma PACs of REM sleep were unaffected, consistent
390 with prior results [20]. Even so, both intra-hippocampal and hippocampal-cortical theta-gamma PAC
391 declined with increasing age in young APP/PS1 mice, suggesting a subtle vulnerability to Aβ
392 amyloidosis.

In plaque-bearing APP/PS1 mice, we previously observed increased synchronization between CA1 cell layer neuron calcium fluctuations and hippocampal theta both online and in REM sleep [18]. Consistent with this result and with the greater vulnerability of online theta-gamma PAC compared to REM sleep in young APP/PS1 mice, synchronization of neuronal calcium with the hippocampal LFP was increased in young APP/PS1 mice in exploratory behavior alone. Although the mechanisms underlying impaired theta-gamma PAC and aberrant synchronization of neuronal calcium levels with the theta oscillation in young APP/PS1 mice remain to be determined, brain oscillations and their coupling are known to reflect the coordinated activity of large populations of excitatory and inhibitory neurons, and imbalanced or uncoordinated excitation and inhibition may contribute. In this context, it is possible that Aβ-mediated dysfunction or loss of inhibitory neurons and synapses may contribute to these findings [64].

Remarkably, the impairment of hippocampal theta-gamma PAC in exploratory behavior predicted the reduction of place cell pairwise reactivation in SWS. This observation raises the possibility of a primary deleterious effect of AβO or other species on memory encoding online, reflected in impaired theta-gamma PAC and hyper-synchronization of neuronal calcium fluctuations with the theta oscillation, that then drives impairment of memory consolidation in SWS. Future experiments will be needed to evaluate this model.

It is noteworthy that the magnitude of impairment of theta-gamma PAC during exploratory behavior observed in young APP/PS1 mice harboring few amyloid plaques was comparable to that observed in 12-month-old mice, where amyloid plaque burden is significant [18]. This observation

416 suggests that plaque burden is unlikely to underlie impairment of theta-gamma PAC in old
417 APP/PS1 mice and implicates the same process. On the other hand, the resilience of theta-gamma
418 PAC in REM sleep in young APP/PS1 mice contrasts with its marked impairment in old APP/PS1
419 mice. Higher concentrations of amyloid-related species and/or the induction of additional
420 pathological processes, such as basal forebrain cholinergic neuron dysfunction and loss [65], may be
421 required to degrade theta-gamma PAC in REM sleep.
422
423 Interestingly, the hippocampal systems level impairments observed here in young APP/PS1 mice
424 precede the behavioral impairments that arise in this AD model on standard behavioral assays,
425 where deficits of contextual memory have been reported to start around 6 months [66,67]. Thus,
426 sampling hippocampal systems level function is likely to provide a sensitive readout for
427 assessment of brain dysfunction and its rescue in AD models.
428
429 Strengths of this study include the evaluation of hippocampal function across the sleep wake cycle
430 of a well-characterized, freely behaving AD model, which unlike anesthetized or behavioral
431 studies, avoids the confounds of anesthesia and links neurophysiological features associated with
432 memory encoding and consolidation. The acquisitions of simultaneous dynamic calcium imaging
433 and local electrophysiological recordings is a further strength, enabling us to connect brain
434 oscillations critical to normal hippocampal mnemonic functions to neuronal calcium fluctuations,
435 place cell activity, and their reactivation in SWS. Limitations of the study include the use of a
436 single model of amyloidosis, and additional work in other models will be informative. A further
437 limitation is the correlative nature of the work. In this regard, future, causal experiments will prove

438 useful to identify the causative factors underlying the hippocampal physiological impairments
439 observed here.
440
441 In summary, the results of this study reveal impairments in hippocampal cellular and oscillatory
442 functions that contribute to memory encoding and consolidation prior to robust Aβ plaque
443 deposition. These findings draw attention away from the Aβ plaque to the pathological
444 contributions of AβO and other Aβ-related species in AD that may help to elucidate and improve
445 upon the significant but, to date, only modest effectiveness of anti-amyloid therapies such as
446 Lecanemab for AD.
447
448 **Methods**
449 All procedures were approved by the Institutional Animal Care and Use Committees of the
450 Massachusetts General Hospital and followed the ethical guidelines of the US National Institutes
451 of Health.
452
453 **Surgical preparation**
454 All procedures were similar to our previous studies [18,65]. Briefly, B6;C3-Tg (APPswe, PSEN1dE9)
455 85Dbo/Mmjax transgenic mice (APP/PS1) mice (Jackson Laboratory) and their age/gender
456 matched non-transgenic control litters were firstly injected with 1 μL AAV-hSyn-GCaMP6f-GFP
457 into the hippocampal CA1 region (AP -2.1 mm, ML -1.65 mm, DV -1.4 mm) under anesthesia
458 (isoflurane 1.5-2%). Two weeks later, a grin lens (1 mm diameter, AP -2.1 mm, ML -1.65 mm,
459 DV -1.4 mm) and a custom drivable probe holding 7 stereotrodes (AP -2.8 mm, ML 2.6 mm, -36
460 º relative to the AP axis, -39 º relative to the inter-aural axis; DV -1.2 mm) were implanted

461 ipsilaterally, to sample the LFP in the vicinity of the calcium imaging site, with cerebellar ground.
462 The microscope baseplate was attached three weeks later. Carprofen (10 mg/kg, s.c) was used for
463 postoperative analgesia. Animals were housed in individual cages with a 12 hr light/12hr dark-
464 standard light cycle. All mice were male to avoid sex differences in Aβ pathogenesis in APP/PS1
465 mice [68].
466
467 **Calcium imaging, electrophysiology, and behavior**
468 The Inscopix^{TM} nVista3 mini-microscope and acquisition system were used to sample calcium
469 imaging at 20 Hz. Local field potential (LFP) (Neuralynx^{TM}) was sampled at 2 kHz followed by
470 0.5-900 Hz filtering. Animal position was recorded with overhead camera tracking of two LED
471 diodes mounted on the headstage. Electrophysiology and calcium imaging were acquired
472 simultaneously, with the latter in 10 min acquisition blocks and 4-5 minute intervals off-camera to
473 avoid photobleaching. Quiet wakefulness (QW), slow-wave sleep (SWS), and REM sleep were
474 acquired immediately after track sessions in the home cage within the same recording room.
475 Exploratory behavior (RUN) was defined when run velocity exceeded 1 cm/sec on the track; QW
476 was defined as wakeful immobility (< 0.5 cm/sec, eyes open) in the home cage; SWS was
477 identified when SWRs were present and delta/theta LFP power ratio exceeded 2, while the animal
478 maintained a sleep posture; REM sleep was identified when the theta/delta LFP power ratio
479 exceeded 2 in sleep.
480
481 **Data analysis.** All analyses were performed using MATLAB (2019b) and were similar to our
482 previous studies [18,65].

483 *Calcium imaging:* Inscopix Data Processing Software (IDPS, Inscopix, Palo Alto, California) was
484 used for movie preprocessing, motion correction, normalization ΔF/F and constrained non-
485 negative matrix factorization (CNMFE) cell identification[69]. The shape and signal-noise-ratio
486 (SNR) of each cell soma was reviewed manually for quality control. Calcium events were then
487 detected at 2 Z scores above the mean, with onset at 30% of peak amplitude. Hypoactivity was
488 defined as < 0.25 transients/min [18,70]; hyperactivity was defined as > 2 Z scores above the mean of
489 the control group for each behavioral state [18].
490 *Place cell analyses:* Spatial tuning curves (3 cm bins) were constructed for each cell for each
491 running direction using all detected calcium events acquired during running. Spatial information
492 was computed and compared to 1000 shuffled spatial information distributions to test significance
493 (Monte Carlo p-value < 0.05) [71]. Place field width was defined at 50% of peak firing distribution
494 over track location [72]. Spike time cross-correlations of all place cell pairs in both online
495 (exploratory/RUN) and subsequent offline (QW, SWS) states were calculated. Reactivation was
496 defined when the same pair was coactivated during both online and specific offline states [45].
497 Coactivation was defined based on the distinguished clusters (cluster 1 not coactivated: <0.001,
498 and cluster 2 coactivated: >0.02) in the distribution of correlations of all place cell pairs in each
499 states (Fig. S1). Results persisted across a broad range of thresholds (between >0.001 and <0.02),
500 here we used >0.002 per previous work [45]. Proportions of reactivated pairs among all pairs of each
501 animal were used to compare between genotypes. Recordings with at least 10 place cells (5 out of
502 7 control mice and 6 out of 8 APP/PS1 mice) were included in the pairwise reactivation analysis.
503 *LFP analyses:* LFPs were filtered to obtain slow oscillations (0.5-1 Hz), delta (1-4 Hz), theta (4-
504 10 Hz), gamma (30-150 Hz), and ripples (100-300 Hz). The spectrograms of each channel were
505 calculated using the Chronux toolbox [73] with a moving window of size 2 s and step size 1 s. A

506 stereotrode in s. radiatum showing high amplitude theta was used for assessments of RUN and
507 REM sleep; a stereotrode in s. pyramidale showing high amplitude SWRs was used for
508 assessments of QW and SWS; a stereotrode within cortex showing slow oscillations and sleep
509 spindles was also used. Power spectra were computed from 0 to 200 Hz using the Chronux toolbox
510 [73], and the sum of relative power of each frequency band was used for quantification. Phase-
511 amplitude-coupling (PAC) modulation index (MI) was calculated with 1-25 Hz for phase
512 frequency and 1-300 Hz for amplitude frequency using the MATLAB toolbox
513 https://data.mrc.ox.ac.uk/data-set/matlab-toolbox-estimating-phase-amplitude-coupling [74,75], and
514 the mean value of the high coupling region was used for quantification [20]. Spindle events were
515 detected at 1.25 Z score with minimum length of 200 ms; SWR events were detected at 3 Z score
516 with minimum length of 20 ms [46]. LFPs were downsampled to the same sampling rate as calcium
517 imaging for the Chronux coherence analysis [73] for oscillatory-cellular synchronization [18].
518

519 **Biochemistry**

520 *Brain protein extraction:* Mice were perfused with cold PBS containing protease inhibitor (cat #
521 A32957), and the brain was rapidly excised. One hemisphere was separated for
522 immunohistochemistry analyses. Cortex and hippocampus were dissected from the remaining
523 hemisphere and immediately frozen in liquid nitrogen, then stored at −80°C before use. Protein
524 extraction was performed as indicated by the ELISA kit. In summary, frozen brain samples were
525 homogenized in 10 vol (w/v) of cold TBS containing protease inhibitor using a Teflon-glass and
526 centrifuged at 16,000 x g for 30 min at 4°C. The pellets were re-suspended in TBS plus 1% Triton
527 X-100 containing protease inhibitor (TBS-T) and centrifuged at 16,000 x g for another 30 min at

528 4°C. The TBS-T fraction was used to measure oligomeric β-amyloid. The total protein
529 concentration in TBS-T fractions was measured using the BCA protein assay kit (cat# 23225).
530 *ELISA:* ELISA was used to quantify oligomeric β-amyloid in cortical and hippocampal samples
531 (Biosensis cat# BEK-2215-1P/2P). Oligomeric β-amyloid concentration was determined using a
532 standard curve, and values are reported as ng/mg of protein. Analyses were blinded to animal age.
533 *Immunohistochemistry:* Hemibrains were drop-fixed in 4% paraformaldehyde for two days and
534 sectioned at 40 mm on a vibratome (Leica, Buffalo Grove, IL). Sections were collected in a 1 in 4
535 series and stored in PBS at 4°C. Sections were mounted, and antigen retrieval was performed with
536 citrate buffer at 95°C for 30 min. Next, sections were blocked and permeabilized in TBS-T with
537 5% bovine serum albumin (BSA) and 5% normal goat serum (NGS) for 1h. Sections were
538 incubated overnight in Alexa Fluor 488 Conjugate primary β-Amyloid antibody (D54D2, cat#
539 51374S) at 4C. Following several washes in PBS, slides were cover slipped with anti-fade
540 mounting media, and images were acquired using an Olympus VS120 Slide Scanner.
541
542 **Statistical analysis**
543 All group values were represented as mean ± s.e.m. For analyses of dynamic calcium imaging
544 hypo- and hyperactivity, mixed effects models were used. For the remaining analyses, Student's
545 *t*-test and one-way ANOVA with repeated measures followed by *post hoc* tests were used for
546 statistical analyses according to the experimental design (SPSS). The significance threshold was
547 set at $p < 0.05$.
548

Data availability

The datasets generated and analyzed in the current study are available in the Dryad repository, https://datadryad.org/stash/share/gN7A2L9rPMErDH74jxAWQUdjKm7A89v4ERaftNsJOiA

Acknowledgements

We thank Joseph J. Locascio for statistical consultation. This work was supported by NIH grants to SNG (R01 AG054551; R01 AG077611).

Competing interests

The authors declare no competing interests.

Reference

1. Bloom, G. S. Amyloid-β and Tau: The Trigger and Bullet in Alzheimer Disease Pathogenesis. *JAMA Neurology* **71**, 505–508 (2014).
2. van Dyck, C. H. *et al.* Lecanemab in Early Alzheimer's Disease. *New England Journal of Medicine* **388**, 9–21 (2023).
3. Mintun, M. A. *et al.* Donanemab in Early Alzheimer's Disease. *N Engl J Med* **384**, 1691–1704 (2021).
4. Budd Haeberlein, S. *et al.* Two Randomized Phase 3 Studies of Aducanumab in Early Alzheimer's Disease. *J Prev Alzheimers Dis* **9**, 197–210 (2022).
5. Honig, L. S. *et al.* Trial of Solanezumab for Mild Dementia Due to Alzheimer's Disease. *N Engl J Med* **378**, 321–330 (2018).
6. O'Keefe, J. Place units in the hippocampus of the freely moving rat. *Experimental Neurology* **51**, 78–109 (1976).
7. O'Keefe, J., Burgess, N., Donnett, J. G., Jeffery, K. J. & Maguire, E. A. Place cells, navigational accuracy, and the human hippocampus. *Philos Trans R Soc Lond B Biol Sci* **353**, 1333–1340 (1998).
8. Cacucci, F., Yi, M., Wills, T. J., Chapman, P. & O'Keefe, J. Place cell firing correlates with memory deficits and amyloid plaque burden in Tg2576 Alzheimer mouse model. *Proceedings of the National Academy of Sciences* **105**, 7863–7868 (2008).
9. Mably, A. J., Gereke, B. J., Jones, D. T. & Colgin, L. L. Impairments in spatial representations and rhythmic coordination of place cells in the 3xTg mouse model of Alzheimer's disease. *Hippocampus* **27**, 378–392 (2017).

10. Belluscio, M. A., Mizuseki, K., Schmidt, R., Kempter, R. & Buzsaki, G. Cross-Frequency Phase-Phase Coupling between Theta and Gamma Oscillations in the Hippocampus. *Journal of Neuroscience* **32**, 423–435 (2012).
11. Colgin, L. L. Rhythms of the hippocampal network. *Nat Rev Neurosci* **17**, 239–249 (2016).
12. Jacobson, T. K. *et al.* Hippocampal theta, gamma, and theta-gamma coupling: effects of aging, environmental change, and cholinergic activation. *Journal of Neurophysiology* **109**, 1852–1865 (2013).
13. Kendrick, K. M. *et al.* Learning alters theta amplitude, theta-gamma coupling and neuronal synchronization in inferotemporal cortex. *BMC Neuroscience* **12**, 55 (2011).
14. Lisman, J. E. & Jensen, O. The Theta-Gamma Neural Code. *Neuron* **77**, 1002–1016 (2013).
15. Tamura, M., Spellman, T. J., Rosen, A. M., Gogos, J. A. & Gordon, J. A. Hippocampal-prefrontal theta-gamma coupling during performance of a spatial working memory task. *Nat Commun* **8**, 2182 (2017).
16. Tort, A. B. L., Komorowski, R. W., Manns, J. R., Kopell, N. J. & Eichenbaum, H. Theta–gamma coupling increases during the learning of item–context associations. *Proc. Natl. Acad. Sci. U.S.A.* **106**, 20942–20947 (2009).
17. Vivekananda, U. *et al.* Theta power and theta-gamma coupling support long-term spatial memory retrieval. *Hippocampus* **31**, 213–220 (2021).
18. Zhou, H. *et al.* Disruption of hippocampal neuronal circuit function depends upon behavioral state in the APP/PS1 mouse model of Alzheimer's disease. *Sci Rep* **12**, 21022 (2022).
19. Prince, S. M. *et al.* Alzheimer's pathology causes impaired inhibitory connections and reactivation of spatial codes during spatial navigation. *Cell Rep* **35**, 109008 (2021).
20. Zhurakovskaya, E. *et al.* Impaired hippocampal-cortical coupling but preserved local synchrony during sleep in APP/PS1 mice modeling Alzheimer's disease. *Sci Rep* **9**, 5380 (2019).
21. Buzsáki, G. Theta Oscillations in the Hippocampus. *Neuron* **33**, 325–340 (2002).
22. Colgin, L. L. Theta–gamma coupling in the entorhinal–hippocampal system. *Current Opinion in Neurobiology* **31**, 45–50 (2015).
23. Arbel-Ornath, M. *et al.* Soluble oligomeric amyloid-β induces calcium dyshomeostasis that precedes synapse loss in the living mouse brain. *Molecular Neurodegeneration* **12**, 27 (2017).
24. Cleary, J. P. *et al.* Natural oligomers of the amyloid-β protein specifically disrupt cognitive function. *Nat Neurosci* **8**, 79–84 (2005).
25. Cline, E. N., Bicca, M. A., Viola, K. L. & Klein, W. L. The Amyloid-β Oligomer Hypothesis: Beginning of the Third Decade. *JAD* **64**, S567–S610 (2018).
26. Ding, Y. *et al.* Amyloid Beta Oligomers Target to Extracellular and Intracellular Neuronal Synaptic Proteins in Alzheimer's Disease. *Frontiers in Neurology* **10**, (2019).
27. Faucher, P., Mons, N., Micheau, J., Louis, C. & Beracochea, D. J. Hippocampal Injections of Oligomeric Amyloid β-peptide (1–42) Induce Selective Working Memory Deficits and Long-lasting Alterations of ERK Signaling Pathway. *Frontiers in Aging Neuroscience* **7**, (2016).
28. Ferreira, S. T., Lourenco, M. V., Oliveira, M. M. & De Felice, F. G. Soluble amyloid-β oligomers as synaptotoxins leading to cognitive impairment in Alzheimer's disease. *Front Cell Neurosci* **9**, 191 (2015).
29. Nicole, O. *et al.* Soluble amyloid beta oligomers block the learning-induced increase in hippocampal sharp wave-ripple rate and impair spatial memory formation. *Sci Rep* **6**, 22728 (2016).

30. Özcan, G. G., Lim, S., Leighton, P. L., Allison, W. T. & Rihel, J. Sleep is bi-directionally modified by amyloid beta oligomers. *eLife* **9**, e53995 (2020).
31. Shankar, G. M. *et al.* Amyloid-β protein dimers isolated directly from Alzheimer's brains impair synaptic plasticity and memory. *Nat Med* **14**, 837–842 (2008).
32. Malinow, R. & Malenka, R. C. AMPA receptor trafficking and synaptic plasticity. *Annu Rev Neurosci* **25**, 103–126 (2002).
33. Yang, T., Li, S., Xu, H., Walsh, D. M. & Selkoe, D. J. Large Soluble Oligomers of Amyloid β-Protein from Alzheimer Brain Are Far Less Neuroactive Than the Smaller Oligomers to Which They Dissociate. *J Neurosci* **37**, 152–163 (2017).
34. Busche, M. A. *et al.* Critical role of soluble amyloid-β for early hippocampal hyperactivity in a mouse model of Alzheimer's disease. *Proc. Natl. Acad. Sci. U.S.A.* **109**, 8740–8745 (2012).
35. Busche, M. A. & Konnerth, A. Neuronal hyperactivity – A key defect in Alzheimer's disease? *BioEssays* **37**, 624–632 (2015).
36. Zarhin, D. *et al.* Disrupted neural correlates of anesthesia and sleep reveal early circuit dysfunctions in Alzheimer models. *Cell Reports* **38**, 110268 (2022).
37. Garcia-Alloza, M. *et al.* Characterization of amyloid deposition in the APPswe/PS1dE9 mouse model of Alzheimer disease. *Neurobiol Dis* **24**, 516–524 (2006).
38. Jankowsky, J. L. *et al.* Mutant presenilins specifically elevate the levels of the 42 residue β-amyloid peptide in vivo: evidence for augmentation of a 42-specific γ secretase. *Human Molecular Genetics* **13**, 159–170 (2004).
39. Takeda, S. *et al.* Brain interstitial oligomeric amyloid β increases with age and is resistant to clearance from brain in a mouse model of Alzheimer's disease. *FASEB J* **27**, 3239–3248 (2013).
40. Zhang, L. *et al.* Dynamic Changes in the Levels of Amyloid-β42 Species in the Brain and Periphery of APP/PS1 Mice and Their Significance for Alzheimer's Disease. *Front Mol Neurosci* **14**, 723317 (2021).
41. Webster, S. J., Bachstetter, A. D. & Van Eldik, L. J. Comprehensive behavioral characterization of an APP/PS-1 double knock-in mouse model of Alzheimer's disease. *Alzheimers Res Ther* **5**, 28 (2013).
42. Jun, H. *et al.* Disrupted Place Cell Remapping and Impaired Grid Cells in a Knockin Model of Alzheimer's Disease. *Neuron* **107**, 1095-1112.e6 (2020).
43. Ego-Stengel, V. & Wilson, M. A. Disruption of ripple-associated hippocampal activity during rest impairs spatial learning in the rat. *Hippocampus* **20**, 1–10 (2010).
44. Ólafsdóttir, H. F., Bush, D. & Barry, C. The Role of Hippocampal Replay in Memory and Planning. *Curr Biol* **28**, R37–R50 (2018).
45. Wilson, M. A. & McNaughton, B. L. Reactivation of Hippocampal Ensemble Memories During Sleep. *Science* **265**, 676–679 (1994).
46. Siapas, A. G. & Wilson, M. A. Coordinated Interactions between Hippocampal Ripples and Cortical Spindles during Slow-Wave Sleep. *Neuron* **21**, 1123–1128 (1998).
47. Born, J., Rasch, B. & Gais, S. Sleep to Remember. *Neuroscientist* **12**, 410–424 (2006).
48. Bazzigaluppi, P. *et al.* Early-stage attenuation of phase-amplitude coupling in the hippocampus and medial prefrontal cortex in a transgenic rat model of Alzheimer's disease. *Journal of Neurochemistry* **144**, 669–679 (2018).
49. Etter, G. *et al.* Optogenetic gamma stimulation rescues memory impairments in an Alzheimer's disease mouse model. *Nat Commun* **10**, 5322 (2019).

50. Gurevicius, K., Lipponen, A. & Tanila, H. Increased Cortical and Thalamic Excitability in Freely Moving APPswe/PS1dE9 Mice Modeling Epileptic Activity Associated with Alzheimer's Disease. *Cerebral Cortex* **23**, 1148–1158 (2013).
51. Stoiljkovic, M., Kelley, C., Stutz, B., Horvath, T. L. & Hajós, M. Altered Cortical and Hippocampal Excitability in TgF344-AD Rats Modeling Alzheimer's Disease Pathology. *Cerebral Cortex* **29**, 2716–2727 (2019).
52. Bandarabadi, M. *et al.* Dynamic modulation of theta-gamma coupling during rapid eye movement sleep. *Sleep* **42**, zsz182 (2019).
53. Montgomery, S. M., Sirota, A. & Buzsáki, G. Theta and Gamma Coordination of Hippocampal Networks during Waking and Rapid Eye Movement Sleep. *J. Neurosci.* **28**, 6731–6741 (2008).
54. Medeiros, R., Baglietto-Vargas, D. & LaFerla, F. M. The role of tau in Alzheimer's disease and related disorders. *CNS Neurosci Ther* **17**, 514–524 (2011).
55. Niikura, T., Tajima, H. & Kita, Y. Neuronal Cell Death in Alzheimer's Disease and a Neuroprotective Factor, Humanin. *Curr Neuropharmacol* **4**, 139–147 (2006).
56. Lambert, M. P. *et al.* Diffusible, nonfibrillar ligands derived from Abeta1-42 are potent central nervous system neurotoxins. *Proc Natl Acad Sci U S A* **95**, 6448–6453 (1998).
57. Lue, L.-F. *et al.* Soluble Amyloid β Peptide Concentration as a Predictor of Synaptic Change in Alzheimer's Disease. *Am J Pathol* **155**, 853–862 (1999).
58. Hampel, H. *et al.* The Amyloid-β Pathway in Alzheimer's Disease. *Mol Psychiatry* **26**, 5481–5503 (2021).
59. O'Brien, R. J. & Wong, P. C. Amyloid precursor protein processing and Alzheimer's disease. *Annu Rev Neurosci* **34**, 185–204 (2011).
60. Joo, H. R. & Frank, L. M. The hippocampal sharp wave-ripple in memory retrieval for immediate use and consolidation. *Nat Rev Neurosci* **19**, 744–757 (2018).
61. Girardeau, G., Cei, A. & Zugaro, M. Learning-Induced Plasticity Regulates Hippocampal Sharp Wave-Ripple Drive. *J. Neurosci.* **34**, 5176–5183 (2014).
62. Atherton, L. A., Dupret, D. & Mellor, J. R. Memory trace replay: the shaping of memory consolidation by neuromodulation. *Trends Neurosci* **38**, 560–570 (2015).
63. Louie, K. & Wilson, M. A. Temporally Structured Replay of Awake Hippocampal Ensemble Activity during Rapid Eye Movement Sleep. *Neuron* **29**, 145–156 (2001).
64. Kurucu, H. *et al.* Inhibitory synapse loss and accumulation of amyloid beta in inhibitory presynaptic terminals in Alzheimer's disease. *European Journal of Neurology* **29**, 1311–1323 (2022).
65. Zhou, H. *et al.* Cholinergic modulation of hippocampal calcium activity across the sleep-wake cycle. *eLife* **8**, e39777 (2019).
66. Lonnemann, N., Korte, M. & Hosseini, S. Repeated performance of spatial memory tasks ameliorates cognitive decline in APP/PS1 mice. *Behavioural Brain Research* **438**, 114218 (2023).
67. Kilgore, M. *et al.* Inhibitors of Class 1 Histone Deacetylases Reverse Contextual Memory Deficits in a Mouse Model of Alzheimer's Disease. *Neuropsychopharmacology* **35**, 870–880 (2010).
68. Li, X. *et al.* Sex differences between APPswePS1dE9 mice in A-beta accumulation and pancreatic islet function during the development of Alzheimer's disease. *Lab Anim* **50**, 275–285 (2016).
69. Zhou, P. *et al.* Efficient and accurate extraction of in vivo calcium signals from microendoscopic video data. *eLife* **7**, e28728 (2018).

70. Lerdkrai, C. *et al.* Intracellular Ca $^{2+}$ stores control in vivo neuronal hyperactivity in a mouse model of Alzheimer's disease. *Proc. Natl. Acad. Sci. U.S.A.* **115**, (2018).
71. Markus, E. J., Barnes, C. A., McNaughton, B. L., Gladden, V. L. & Skaggs, W. E. Spatial information content and reliability of hippocampal CA1 neurons: Effects of visual input. *Hippocampus* **4**, 410–421 (1994).
72. Go, M. A. *et al.* Place Cells in Head-Fixed Mice Navigating a Floating Real-World Environment. *Frontiers in Cellular Neuroscience* **15**, (2021).
73. Bokil, H., Andrews, P., Kulkarni, J. E., Mehta, S. & Mitra, P. P. Chronux: A platform for analyzing neural signals. *Journal of Neuroscience Methods* **192**, 146–151 (2010).
74. Onslow, A. C. E., Bogacz, R. & Jones, M. W. Quantifying phase–amplitude coupling in neuronal network oscillations. *Progress in Biophysics and Molecular Biology* **105**, 49–57 (2011).
75. Osipova, D., Hermes, D. & Jensen, O. Gamma Power Is Phase-Locked to Posterior Alpha Activity. *PLoS ONE* **3**, e3990 (2008).